Liu et al. Nanoscale Research Letters (2017) 12:558
DOI 10.1186/s11671-017-2329-9

Nanoscale Research Letters

NANO EXPRESS Open Access

Large-Area WS_2 Film with Big Single Domains Grown by Chemical Vapor Deposition

Pengyu Liu, Tao Luo, Jie Xing*, Hong Xu, Huiying Hao, Hao Liu and Jingjing Dong

Abstract

High-quality WS_2 film with the single domain size up to 400 μm was grown on Si/SiO_2 wafer by atmospheric pressure chemical vapor deposition. The effects of some important fabrication parameters on the controlled growth of WS_2 film have been investigated in detail, including the choice of precursors, tube pressure, growing temperature, holding time, the amount of sulfur powder, and gas flow rate. By optimizing the growth conditions at one atmospheric pressure, we obtained tungsten disulfide single domains with an average size over 100 μm. Raman spectra, atomic force microscopy, and transmission electron microscopy provided direct evidence that the WS_2 film had an atomic layer thickness and a single-domain hexagonal structure with a high crystal quality. And the photoluminescence spectra indicated that the tungsten disulfide films showed an evident layer-number-dependent fluorescence efficiency, depending on their energy band structure. Our study provides an important experimental basis for large-area, controllable preparation of atom-thick tungsten disulfide thin film and can also expedite the development of scalable high-performance optoelectronic devices based on WS_2 film.

Keywords: Two-Dimensional Materials, Tungsten Disulfide, Chemical Vapor Deposition (CVD), Transition Metal Dichalcogenides (TMDCs)

Background

Two-dimensional materials have important research significance in the future electronics and optoelectronics because of their unique planar advantages, quantum confinement effect, and lack of interlayer interference. As a typical two-dimensional material, graphene possesses many outstanding properties, such as super high carrier mobility, excellent thermal conductivity, outstanding flexibility, and ultrafast photoresponse, which have presented as a promising material in a wide range of application fields of next-generation flexible electronics, optoelectronics, and energy storage [1]. Massless Dirac fermions endow graphene with ultrahigh carrier mobility, but its semi-metallic property with zero bandgap greatly limits its use in devices. In recent years, the graphene-like monolayer transition metal dichalcogenides have aroused widespread interest in the scientific community and become a research focus in semiconductor micro- and nanoelectronics due to its moderate bandgap, excellent carrier mobility, and tunable electrical and optical properties.

Two-dimensional transition metal dichalcogenides (2D TMDCs) usually have a generalized chemical formula as MX_2, where M is a transition metal of groups 4–10 (Mo, W, etc.) and X is a chalcogen (S, Se, Te, etc.). MX_2 is a typical layered compound, every unit cell of which contains three layers of atoms (X-M-X). The intralayer atoms are tightly bound with covalent bonds, and the interlayer atoms are coupled by weak van der Waals force [2]. Similar to MoS_2, monolayer WS_2 has many novel physical properties distinguished from its bulk, such as direct bandgap, strong spin-orbit coupling, and intense interaction between light and matter. Therefore, it has promising potential application in future optoelectronic and micro/nanoelectronic devices [3]. So far, several routes of fabricating single-layer two-dimensional materials have been established, such as mechanical exfoliation, film sulfurization, thermal decomposition, and chemical vapor deposition. Among them, mechanical exfoliation suffers from the drawbacks of low yield, poor

* Correspondence: xingjie@cugb.edu.cn
School of Science, China University of Geosciences, Beijing 100083, China

repeatability, and limited size [4]. In film sulfurization, a thin W or WO_3 film is firstly sputtered on the substrate, and then, the W/WO_3 film is sulfurized in sulfur-vapor atmosphere. The process is relatively simple, but the thickness of the film is difficult to control [5–7]. Liu et al. synthesized MoS_2 films by thermal decomposition. After being soaked in $(NH_4)_6MoS_4$ solution, the substrate was taken out and heated at 500 °C in an Ar/H_2 atmosphere. Finally the WS_2 film with a large area and a uniform thickness was obtained; however, the crystalline quality of the films was poor [8]. Chemical vapor deposition (CVD) has become an important and widely used technique for growing two-dimensional TMDC materials due to its easy operation, good controllability, relatively mature fabrication routes, and high yield of large-area few-layer film [9–13].

Since 2011, many research groups in the world successfully have synthesized atom-thick WS_2 films by the CVD method. Zhang et al. synthesized the atomic-layered triangular WS_2 film on sapphire substrate by low-pressure chemical vapor deposition with single domain size up to 50 μm [14]. Cong et al. improved the CVD method by putting a single-end-sealed smaller-diameter quartz tube inside a bigger-diameter quartz tube and sandwiching a trace of WO_3 powder between two wafers. This method effectively increases the precursor concentration and pressure in the tube, and the obtained single-domain size was up to 178 μm [3]. Considering that the WO_3 precursor has a high sublimation temperature, Li et al. introduce a proper amount of alkali metal halides in chemical vapor deposition reaction as growth promoters. Alkali metal halide (MX, M=Na or K, X=Cl, Br or I) could reduce the reaction temperature by about 100 °C through forming volatile tungsten oxyhalide species, which facilitated the delivery of the precursor to the growth substrate. However, the addition of alkali halide in reaction tube inevitably introduces impurities and pollutes the reaction products [15]. Both Yanfeng Zhang's and Kyung Nam Kang's group reported that adding an appropriate concentration of H_2 contributes to the rapid sublimation and sulfurization of WO_3 precursor, because the reducibility of H_2 is stronger than that of S [14, 16]. Fu et al. studied the effects of gas flow rate and reaction temperature on the morphology and domain size of WS_2 films in an argon-hydrogen mixture (97%Ar + 3%H_2) atmosphere. They got 52 μm WS_2 flakes by optimizing the CVD growth conditions [17]. Rong et al. used a two-temperature-zone furnace to precisely control sulfur introduction time to achieve an ideal large-area WS_2 film growth with single domain size up to 370 μm [18]. Although CVD method has many advantages, it is still urgent and very challenging to coordinate the intricate and complicated relationship among many growth parameters. At present, arising from the high sublimate temperature of WO_3 precursor and the potential danger in using Ar and H_2 gas mixtures during growth, the preparation of high-quality WS_2 films with large domain size still faces great challenges. In this work, we did a systematic and deep study on the growth rules of WS_2 films synthesized by CVD technique. For the first time, we investigated comprehensively the impact of different growing parameters on the morphology of WS_2 films, such as precursor types, gas pressure, growing temperature, holding time, the amount of sulfur powder, gas flow rate, and substrate position. By optimizing the processing conditions, large-area WS_2 films with big single domains were obtained via an atmospheric-pressure chemical vapor deposition (AP-CVD) method. The films were examined by Raman, atomic force microscopy (AFM), transmission electron microscopy (TEM), and photoluminescence (PL) measurements to have an excellent crystalline quality. Our study paves a way to fabricate large monolayer WS_2 single crystal with excellent properties, which is critical to building scalable devices.

Methods

To synthesize WS_2 film, WO_3 (Sigma-Aldrich, 99.9%), $WO_{2.9}$ (Alfa Aesar, 99.99%) and S (Alfa Aesar, 99.0%) powders were used as W and S precursors, respectively. In a typical growth process, a single-side-polished SiO_2/Si wafer was firstly cleaned in ethanol, isopropanol, and deionized water in sequence by ultrasonic cleaning for 15 min. A small amount of tungsten oxide powder (0.1 g) was uniformly spread on the bottom of a crucible, and the Si wafer with a thickness of 300 nm SiO_2 was put upside down with the polished side facing towards the tungsten oxide powder. Then, the crucible was located at the center of quartz tube (60 mm in diameter) as shown in Fig. 1a. The quartz boat with sulfur powder inside was placed in the upstream region of the quartz tube and warmed up by the radiation heat of the tube furnace. After the quartz tube was pumped down to a pressure of 100 mTorr, the quartz tube was purged using Ar gas at 500 sccm for 30 min, and then, the Ar gas was controlled at a constant flow rate until the reaction was finished. The furnace was heated firstly from room temperature to 150 °C and dwelled at this temperature for 20 min to remove moisture in the tube. Then, the temperature continued to increase to the desired value with a heating rate of 10 °C/min. After reaching the growth temperature, the furnace kept the temperature for a period of time. At the end of the growth process, the quartz tube was cooled down to room temperature naturally. To be clear, the whole temperature control scheme is shown in Fig. 1b.

The morphologies of as-grown WS_2 flakes were characterized by a Hitachi S4800 scanning electron microscope with an acceleration voltage of 5–10 kV. Raman

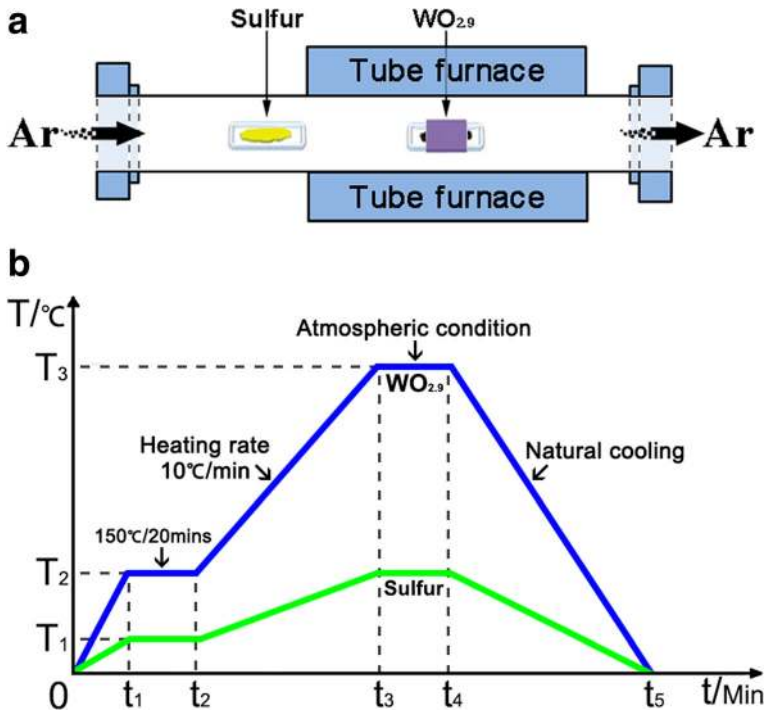

Fig. 1 **a** The schematic setup of CVD furnace. **b** The heating and cooling curves of $WO_{2.9}$ and S powder

measurements were conducted using Nanophoton Raman-11 microscope with an ultra-high speed imaging capability. The Si peak at 520 cm^{-1} was used as a reference for wavenumber calibration. Steady-state PL spectra were taken by a confocal micro-PL system. A 532-nm excitation laser was focused on the sample by using a large numerical aperture objective with a spot size around 1–2 μm in diameter. Topography images of the sample were obtained by using atomic force microscope (Bruker multimode 8) in tapping mode. A field emission JEOL JEM-2100F was operated at 200 kV for high-resolution TEM (HRTEM) and selected-area electron diffraction (SAED) imaging.

Results and Discussion

In CVD synthesis, the growth of two-dimensional TMDCs is impacted by many factors, such as pressure, temperature, gas flow rate, and growing time. These factors are very important in the growth of high-quality and large-area 2D WS_2 film. In this paper, the influence of each of these factors on the morphology of WS_2 films is firstly discussed in detail, and then, the optimum growth conditions for large-area few-layer films are determined. Finally, in order to examine the films' structure and crystal quality, the characterization results under the optimized experimental conditions are presented, including Raman, AFM, PL, and TEM.

WO_3 and $WO_{2.9}$

We used WO_3 and $WO_{2.9}$ powder as two distinct precursors to investigate their effects on the growth of WS_2 film. Fig. 2a, b shows SEM images of WS_2 films grown with precursors of WO_3 and $WO_{2.9}$, respectively. When WO_3 was used as W source, it was hardly to see WS_2 film on the substrate, which was further confirmed by Raman measurements. However, when $WO_{2.9}$ was used as precursor, there appeared a large number of triangular WS_2 domains on the substrate. After dozens of repeated experiments, we found that the yield of triangular WS_2 with $WO_{2.9}$ precursor was much higher than that in the case of WO_3 as precursor. The reproducibility of this experiment result was over 90%. van der Vlies et al. have studied the basic reaction steps in the sulfidation of WO_3 crystal [19]. They found that W^{6+} cannot be directly sulfurized by S unless some intermediates are formed due to the high W–O bond energy. The reduction of W^{6+} to W^{5+} is mandatory for an incorporation of sulfur in the WO_3 lattice. For $WO_{2.9}$ in our case, its partial W^{6+} ions have been reduced to W^{5+} or W^{4+} ions. Therefore, we think the substitution of W^{5+} or W^{4+} for W^{6+} at the initial stage facilitates the growth of the single crystal WS_2 film.

Tube Pressure

For this study, we adopted two pressure values during the growth of WS_2 film in experiments: low pressure

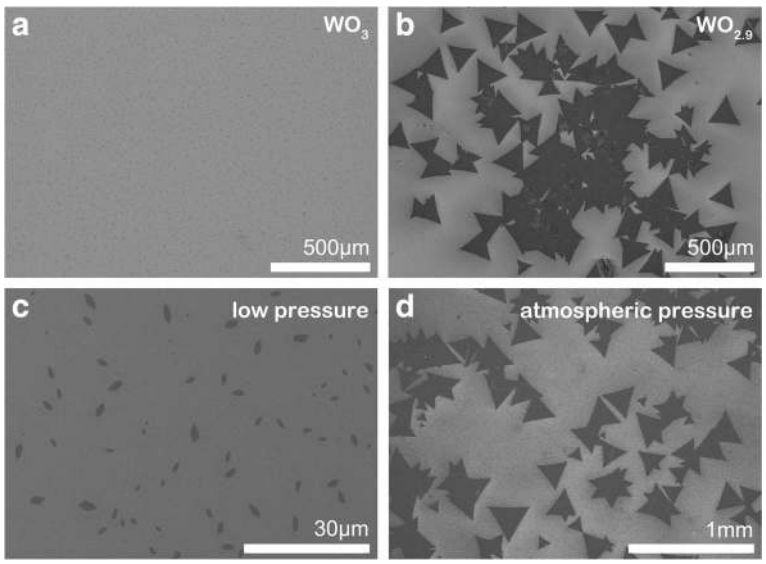

Fig. 2 **a**, **b** The SEM images of WS_2 films prepared using WO_3 and $WO_{2.9}$ as W source, respectively. **c**, **d** The SEM images of WS_2 samples prepared at low pressure and one atmospheric pressure, respectively

(< 100 mTorr) and one atmospheric pressure (1 atm). Figure 2c shows a SEM image of the sample prepared under a low-pressure environment. As we found, only leaf-like flakes were randomly distributed over the substrate, which were not WS_2 but WO_3, as was further confirmed by Raman characterization. Figure 2d shows a SEM image of the sample grown under one atmospheric pressure. In contrast with Fig. 2c, there were many triangular domains with size above 100 μm appearing on the substrate, which were WS_2 as evidenced by Raman spectroscopy. Such contrast experiments have been repeated many times, and every time, we got almost the same results. Compared with low-pressure mode, atmospheric pressure mode was more helpful to get a high yield of WS_2 flakes with large size and clear edges. As we know, CVD process generally includes two stages: (1) gas transportation and gas phase reaction and (2) surface adsorption and surface reaction. In both these two stages, collision process is a very important and robust factor. At one atmospheric pressure, the mean free path of gas molecules becomes shorter and the collision frequency gets higher (see Additional file 1). The higher collision frequency combined with high temperature and high flow rate usually lead to a higher reaction rate and a higher nucleation rate by promoting the chemical reaction between precursors or between precursor clusters and substrate. On the other hand, from the theory of thermodynamics, the chemical free-energy change ΔG (< 0) is the driving force for nucleation. The critical free-energy change ΔG^* could be regarded as an energy barrier of nucleation, which is inversely correlated with the gas pressure [20]. Therefore, the higher pressure in APCVD always leads to a smaller nucleation energy barrier, a higher nucleation rate, and a larger nucleation density than those in the case of low pressure CVD (LPCVD). So, the atmospheric pressure mode in our experiments is more favored in growing 2D TMDC films.

Growth Temperature

Based on the above results, we chose $WO_{2.9}$ as W source and adjusted the tube pressure as one atmospheric pressure. In the following, we investigate the influence of growth temperature on the crystalline quality of WS_2 film. We conducted a series of experiments by varying the furnace temperature at 750, 800, 850, 880, 900, and 950 °C, respectively. As shown in Fig. 3, with increasing temperature, the average domain size of WS_2 films first increased and then decreased. Low temperature induced low diffusion rate of the precursor, so that the precursor can be readily trapped at pregrowth sites on the substrate. At the very early precursor nucleation stage, most nucleation sites formed trap centers and the subsequent precursor nucleated at those trapping sites (Fig. 3b). As a result, many spot-like WS_2 domains were obtained. With raising temperature, the formation of new phases became more difficult due to the increased critical nucleus radius and the boosted nucleation free energy barrier, which restrained nucleation and deposition of WS_2 on the substrate, resulting in a decreased nucleation density. At the same time, the molecular thermal kinetic energy increased significantly,

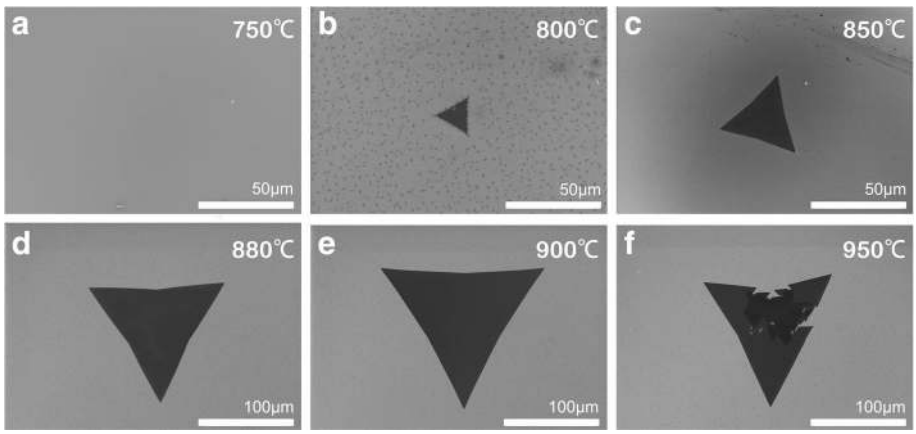

Fig. 3 The SEM images of WS_2 samples prepared at 750 °C (**a**), 800 °C (**b**), 850 °C (**c**), 880 °C (**d**), 900 °C (**e**), and 950 °C (**f**), respectively

which facilitated the surface diffusion of WO_{3-x} and the reaction of WO_{3-x} with S. Thus, it is in line with better crystallization of WS_2 lattices and increased flake size (Fig. 3c–e). However, when the growth temperature was further raised to 950 °C, the overall flake did not grow larger but slightly smaller, and some flakes exhibited some cracks during growth as shown in Fig. 3f. We conjecture the cracks may happen at the sites of grain boundaries or defects, where the chemical bond is relatively fragile and easy to be broken up by high temperature.

Holding Time

In this section, the holding time in our experiments was controlled at 5, 10, 20, and 30 min, respectively. The growth temperature was set as 900 °C, and the amount of S powder was fixed at 0.7 g. As shown in Fig. 4, with the increase of the holding time, the domain size of the films expanded continuously, from about 30 μm at 5 min to about 120 μm at 10 min. However, the lateral size did not continue to enlarge further for the holding time of 20 min or even 30 min. We speculate that it might be related with multiple factors, for example, the substrate surface roughness, nucleation density, and gas molecular diffusion rate. From the thermodynamics theory, the change of free energy during growing may also determine or even limit its lateral size. Additionally, the existing complete triangular film would inevitably suffer from frequent impingement from surrounding gas molecules, which may pollute or even destroy the original film, causing defects in the films. These defects may keep spreading at high temperature and finally damage the original complete film, as shown in Fig. 4d.

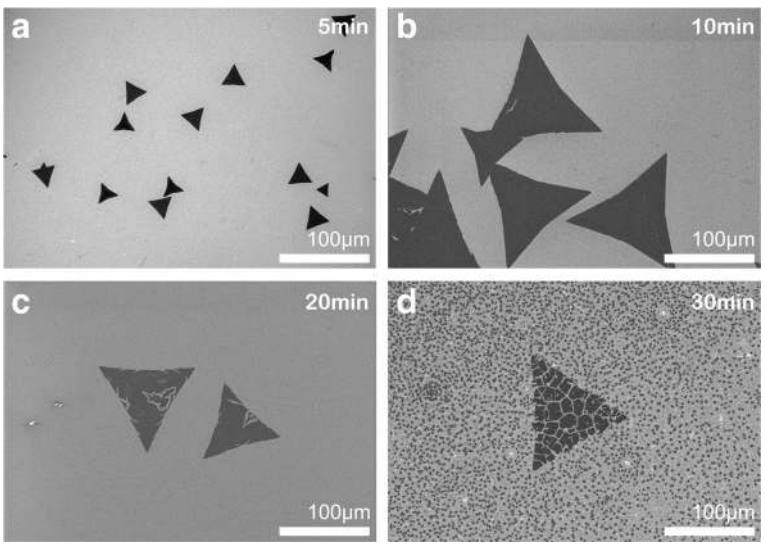

Fig. 4 The SEM images of WS_2 films prepared at 5 min (**a**), 10 min (**b**), 20 min (**c**), and 30 min (**d**), respectively

The Amount of the Sulfur Powder

The amount of the sulfur powder used in growth is also a very important factor. Although the growth dynamics of two-dimensional materials are not fully understood, yet, it is generally accepted that two possible growth modes dominate in the 2D TMDC material growth: (1) MO_{3-x} species adsorb and diffuse on the surface of the substrate as well as react with sulfur vapor atoms to form MS_2; (2) MO_{3-x} groups react directly with S atoms in gas phase, and the resulting MO_xS_y clusters adsorb, nucleate, and grow on the substrate. Clearly, these two modes should be in direct competition depending on the sulfur concentration in the environment. In our experiments, we loaded the amount of sulfur powder as 0.3, 0.5, 0.7, and 0.9 g, respectively, in order to study the influence of the S vapor concentration on the growth of WS_2 film. When the sulfur powder was only 0.3 g, the partial pressure of sulfur vapor in quartz tube was relatively low, which easily produced incompletely sulfurized film. As shown in Fig. 5a, in addition to few triangular WS_2 flakes with size around 30 μm, there were many small irregular-shaped spots (edge size < 5 μm). These small spots were checked by Raman spectroscopy and proved not to be WS_2. With the sulfur powder addition from 0.5 to 0.7 g, a large number of triangle-shaped WS_2 domains appeared on the substrate, and their average size increased from ~ 50 μm to over 100 μm (Fig. 5b, c). When the sulfur powder was further added up to 0.9 g, larger domains with ~ 300 μm edge length and many small particles were present on the substrate, as shown in Fig. 5d. Analyzed by energy-dispersive spectroscopy (EDS) measurement (see Additional file 1), most of these small particles were WO_xS_y grains, acting as seed nuclei and constantly reacting with S atoms to form WS_2 flakes [21]. The adjacent flakes with the same crystalline orientation grew up with time and finally merged into a larger domain. It is easy to see in Fig. 5d that the large triangular domain was obviously made up of many smaller triangular domains. Under high sulfur partial pressure, the number of crystal nuclei increased significantly. Adjacent nuclei grew competitively, and at the same time, their crystal orientations became disordered, resulting in a rough edge. Feldman et al. claimed that the high S partial pressure can lead to WO_{3-x} nanoparticles wrapped up by a layer of WS_2 inorganic fullerene structure [22, 23], which would suppress the further reaction between the WO_{3-x} core and the outer sulfur atoms. So, we could see some particles remaining on the film surface. It should be noted that with the adding of the sulfur powder, the edges of triangular-like flakes became more concave, which is possibly caused by the markedly different growth rate of the S zigzag (S-zz) edges and the W zigzag (W-zz) edges [24]. In sum, the experimental results presented here reveal that loading a proper amount of sulfur powder plays a critical role in the growth of high-quality two-dimensional WS_2 films.

Gas Flow Rate

In this part, we set gas flow rates as 50, 100, 120, 140, 160, and 180 sccm, respectively, to explore the influence of gas flow rate on film growth. Other growth conditions were regulated as the aforementioned optimized parameter. As shown in Fig. 6, when the flow rate of Ar increased from 50 to 180 sccm, WS_2 domains experienced a morphology transformation as well as a size change. For the gas flow rate of 50 sccm, the WS_2 film was dominated by ~ 40 μm truncated triangular domains. As the flow rate increased from 50 to 120 sccm, the truncated

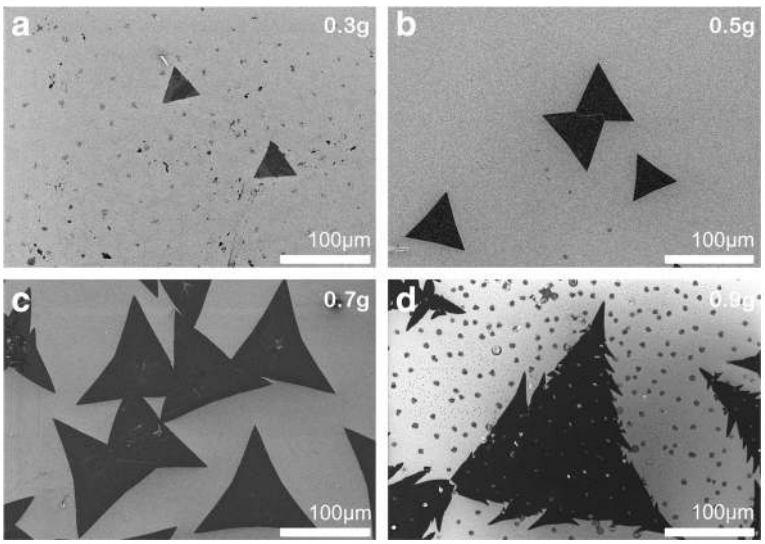

Fig. 5 The SEM images of WS_2 films grown under different sulfur quantities: 0.3 g (**a**), 0.5 g (**b**), 0.7 g (**c**), and 0.9 g (**d**), respectively

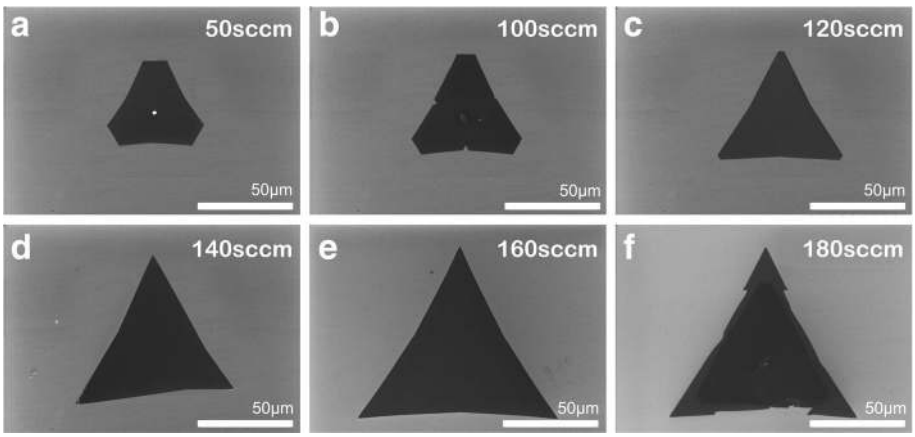

Fig. 6 The SEM images of WS_2 films prepared at different Ar gas flow rates: 50 sccm (**a**), 100 sccm (**b**), 120 sccm (**c**), 140 sccm (**d**), 160 sccm (**e**), and 180 sccm (**f**), respectively

side became shorter and shorter, and finally, the flakes turned into a triangular shape with sharp and smooth edges. At the same time, the average domain size was obviously enlarged to ~ 60 μm. Then, the domains stop to change their shape and continued to grow to ~ 100 μm at a flow rate of 160 sccm. When the gas flow rate reached 180 sccm, no further increase in size was observed. As we know, WS_2 bulk has a trigonal prismatic crystal structure (2H phase), where each W atom is prismatically coordinated to six surrounding S atoms, forming a thermodynamically stable phase. We assume that all shapes of domains start growing from a hexagonal nucleus with three sides of W zigzag (W-zz) terminations and another three sides of S zigzag (S-zz) terminations. As the gas flow rate increased, more S vapor atoms were brought to the center of the quartz tube and induced a smaller Mo to S atomic concentration ratio. Warner et al. investigated the influence of Mo/S atom ratio on the morphology of MoS_2 films based on the principle of crystal growth [24]. According to their work, when the W:S atom ratio gradually changed to less than 1:2, three W-zz terminations grew faster than another three S-zz terminations, which would result in the domain shape transformation from hexagon into truncated triangle and finally into equilateral triangle. Also, the high flow rate promoted the mass transfer process, which contributed to the increase in the crystal growth rate. As the gas flow rate was further raised from 160 to 180 sccm, instability may occur as atoms did not have enough time to move to the right lattice locations, and the probability of defect formation and anisotropy of growth increased owing to the local thermal disturbance and the local imbalance of precursor concentration and pressure. Therefore, at high gas flow rate, the smooth edges of WS_2 films are easy to get rough as shown in Fig. 6f.

The Position of Substrate

Last but not the least, the position of substrate was also a key parameter to WS_2 growth. Here, we make a comparison between two substrate positions. Substrate A was placed above the alumina boat and faced down the tungsten oxide powder, and substrate B was positioned at the downstream as shown in Fig. 7a. At the position of the tube center, the higher temperature determined a higher supersaturated concentration of the precursor, which always led to a smaller crystallization nucleus density. At the same time, due to sufficient precursor supply and high atomic diffusion rate, it was easier to grow large-area WS_2 single domains (~ 200 μm) on substrate A. In contrast, for substrate B placed at the downstream, the lower temperature resulted in a reduced supersaturation of the precursor, which easily brought about more nuclei appearing on the substrate. Meanwhile, owing to the low precursor concentration and low molecular kinetic energy, the single domains on substrate B (~ 10 μm) grow much smaller than those on substrate A, as is shown in Fig. 7b, c.

Optimization and Characterization

In preceding work, a series of experiments have been carried out to investigate the impacts of the growth parameters on the morphology evolution of WS_2 film, including growing temperature, holding time, gas flow rate, and the quantity of sulfur. Our results enable us to realize controllable monolayer WS_2 growth and also provide some general guidelines for other 2D material growth. Based on the above experiment results, we obtained the optimal experimental conditions for the growth of high-quality large-area WS_2 film: 0.1 g $WO_{2.9}$ and 0.7 g S powder are taken as W and S precursors, respectively; the substrate is located right above the alumina boat facing down the $WO_{2.9}$ powder; the growth

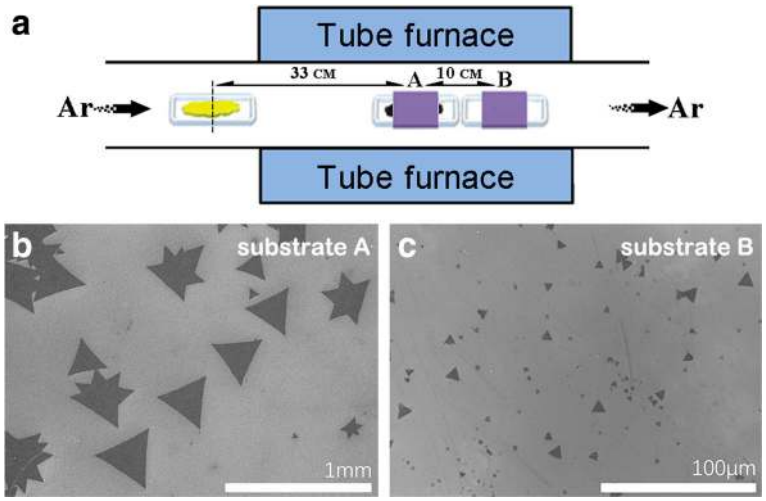

Fig. 7 **a** The schematic experimental setup with the position of substrates A and B. **b**, **c** The SEM images of synthesized WS_2 films on substrates A and B, respectively

temperature is controlled at 900 °C and kept for 10 min; the Ar gas flow rate is set as 160 sccm with tube pressure maintaining at one atmospheric pressure. Figure 8a shows a SEM image of a typical WS_2 single domain synthesized under the optimized condition. The domain has a complete and regular triangular shape with sharp and smooth edge length of ~ 400 μm, which is much bigger than the edge size of WS_2 domain prepared by micromechanical exfoliation.

Raman spectroscopy has been widely used to study 2D materials, from which the information of molecular vibration and rotation in the material can be extracted. So, it offers a fingerprint spectrum to be used to identify the structure of the material. Figure 8b exhibits a typical Raman mapping of a WS_2 film constructed by plotting A_{1g} mode intensity, which clearly shows a perfect triangular shape. Figure 8c shows Raman spectra of the three different areas marked by colored boxes in Fig. 8b over a frequency range of 100–900 cm^{-1}. The measurement was performed at room temperature with 532 nm laser excitation. In addition to the Raman peak at 520 cm^{-1} from substrate Si, the two distinct peaks at ~ 352.5 and ~ 419 cm^{-1} denote typical WS_2 optical phonon vibration modes E^1_{2g} and A_{1g}. These two modes correspond to the in-plane and out-of-plane vibrations of WS_2 lattice, respectively, which are shown in Fig. 8d. With decreasing film thickness, the A_{1g} peak is redshifted, and concurrently, the E^1_{2g} mode is blueshifted due to the weakened interlayer interaction, leading to a decrease in the frequency separation between the two modes. Therefore, the frequency separation is often used to identify the thickness of the two-dimensional material. For the left WS_2 single domain labeled with blue box (Fig. 8b), the Raman frequency difference of the E^1_{2g} and A_{1g} mode is around 71 cm^{-1}, where the two peaks' intensity ratio (A_{1g}/E^1_{2g}) is about 0.5, as shown in Fig. 8c. The high intensity of the A_{1g} peak confirms the two- to three-layered structure of the crystal. For the right WS_2 flake labeled with green box, the Raman frequency interval reduces to 67 cm^{-1}, and the intensity ratio of the two peaks is about 0.21. At the same time, the significant reduction in the intensity of A_{1g} peak than that of the E^1_{2g} peak confirms a monolayer WS_2 [25].

Atomic force microscopy (AFM) is an effective tool to measure the surface topography of materials by "touching" the sample surface with a mechanical probe. The information of the WS_2 film thickness can be obtained directly by AFM measurement. A height image of a WS_2 single domain and the line profile across the flake clearly show a height of 0.82 nm (Fig. 8e), which is in the height range of a single-layer WS_2 film and consistent with the results reported in the literatures [10, 14].

To study the details of light emission from the CVD WS_2 flakes, micro-photoluminescence (m-PL) spectroscopy measurement and PL intensity mapping were performed (with 532 nm laser excitation). As shown in Fig. 8f, the PL intensity of monolayer WS_2 is much stronger than that of multilayer. It is well known that the electronic band structure transitions from indirect to direct bandgap as WS_2 is thinned down from multilayer to monolayer. Strong emission is observed only for the monolayer. Furthermore, the strong PL peak located at 627 nm is in agreement with the reported direct bandgap of ~ 2 eV [26, 27]. The full width at half maximum (FWHM) value of ~ 47 meV is close to those from mechanically exfoliated monolayers in previous reports [28, 29]. Figure 8g shows the PL intensity image of the triangular WS_2

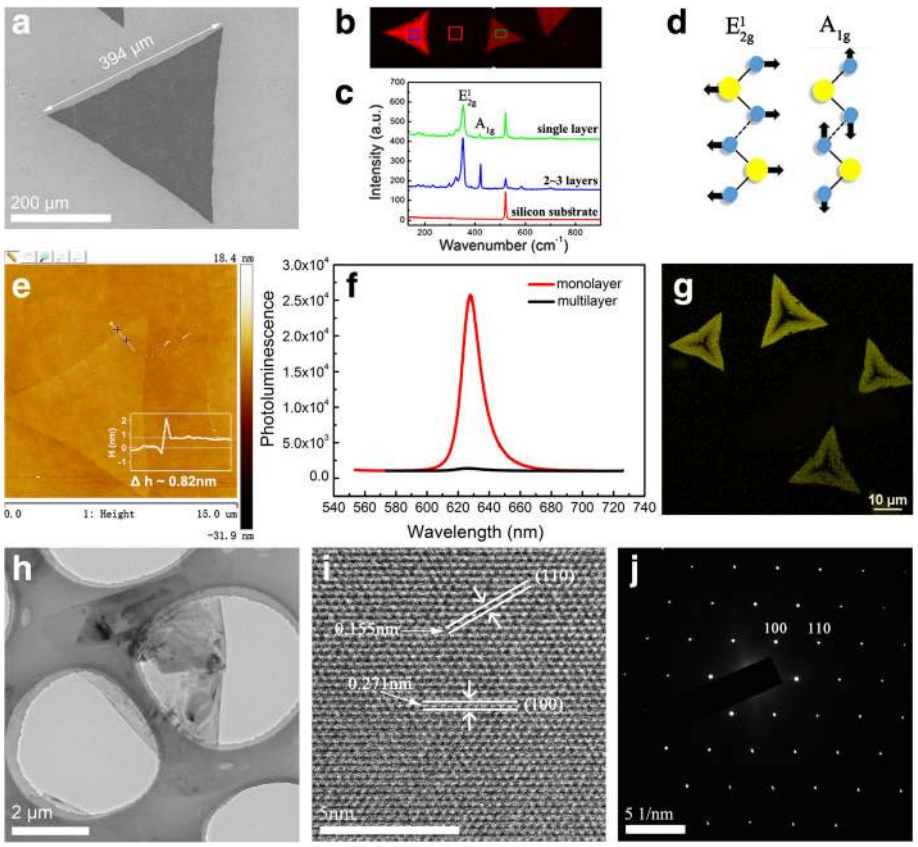

Fig. 8 **a** The SEM image of synthesized WS_2 film. **b**, **c** Raman mapping and the corresponding Raman spectra of WS_2 flakes. **d** The schematic of two typical Raman vibration modes E^1_{2g} and A_{1g}. **e** An AFM image and height profile for a WS_2 single domain. **f** The PL spectra of a monolayer and a multilayer WS_2 flake. **g** Fluorescent image of monolayer WS_2 flakes. **h** TEM image of a WS_2 flake on a copper grid. **i**, **j** High-resolution TEM image and its corresponding SAED pattern of the freely suspended monolayer WS_2 on a TEM grid

monolayer, which exhibits non-uniform emission intensity across the flakes. The edges emit the brightest light, and the strength of the emission gradually decays when moving towards the body center and eventually becomes invisible. Similar results have been reported in other papers [3, 26]. Cong et al. explained the suppressing of PL at the center might be due to the existence of structural and charge defects. For instance, S vacancies are inevitably induced in CVD growth of WS_2 films. The related lattice defects and dislocations could become the non-irradiative recombination centers for excitons, which could result in heavily reduced PL emission intensity.

Finally, we utilized TEM and SAED to evaluate the crystallinity of WS_2 flakes. Figure 8h gives a typical low-magnification TEM image of a triangular WS_2 flake on a holy carbon-coated copper grid. The flake was broken during transfer process, but we still can clearly see that the surface of the film is clean, free from other contaminants. The HRTEM image (Fig. 8i) reveals the hexagonal ring lattice consisting of alternating tungsten atoms and sulfur atoms. The corresponding SAED pattern further confirmed its hexagonal symmetry. The first-order diffraction spots, corresponding to (100) planes, were used to calculate the interspacing d of (100) planes. We found that d (100) equals to 0.271 nm, which is in agreement with the results deduced from HRTEM measurement. Also, the interspacing d (110) is deduced to be 0.155 nm according to the (110) diffraction spots in SAED pattern. Both interplanar distances coincide well with those of bulk WS_2 [14].

Conclusions

We systematically investigated the influence of various synthesis parameters on the morphology evolution of WS_2 film grown by chemical vapor deposition, such as precursors, pressure, growth temperature, holding time, amount of sulfur powder, gas flow rate, and source-substrate distance. Based on the optimized experimental conditions, large-area WS_2 thin films with single domain size up to ~ 400 μm have been successfully prepared on Si/SiO_2 wafer. The crystal structure, layer number, and luminescence of the WS_2 films have been examined by Raman spectra, transmission electron microscopy, atomic

force microscopy, and photoluminescence. We believe our results will lead to further progress in improving the crystalline quality and large-area growth of the exciting 2D transitional metal dichalcogenides (TMDCs). At the same time, this work will push forward the applications of TMDC film in the fields of micro-(nano-) optoelectronics, photovoltaic industry, photocatalysis, and energy storage.

Additional file

Additional file 1: Supplementary material for WS_2 film. **Figure S1.** SEM pictures of WS_2 flakes synthesized from different batches. **Figure S2.** SEM pictures of WS_2 films before (a) and after (b) being annealed at 950 °C under Ar atmosphere. (DOCX 2790 kb)

Abbreviations

2D: Two-dimensional; AFM: Atomic force microscopy; APCVD: Atmospheric pressure chemical vapor deposition; EDS: Energy-dispersive spectroscopy; FWHM: Full width at half maximum; LPCVD: Low pressure chemical vapor deposition; PL: Photoluminescence; SAED: Selected-area electron diffraction; SEM: Scanning electron microscopy; TEM: Transmission electron microscopy; TMDCs: Transition metal dichalcogenides

Acknowledgements

This work has been supported by the National Natural Science Foundation of China (Grant Nos. 11104255) and Fundamental Research Funds for the Central Universities.

Authors' Contributions

XJ and LPY initiated the research and analyzed the experimental data. LPY, LT, and XH worked on the growth and characterization of the CVD thin films. XJ, HHY, LH, and DJJ discussed the experimental results. XJ wrote the manuscript. All authors read and approved the final manuscript.

Competing Interests

The authors declare that they have no competing interests.

Publisher's Note

Received: 28 June 2017 Accepted: 26 September 2017
Published online: 03 October 2017

References

1. Novoselov KS, Geim AK, Morozov SV, Jiang D, Zhang Y, Dubonos SV, Grigorieva IV, Firsov AA (2004) Electric field effect in atomically thin carbon films. Science 306:666–669
2. Wang QH, Kalantar-Zadeh K, Kis A, Coleman JN, Strano MS (2012) Electronics and optoelectronics of two-dimensional transition metal dichalcogenides. Nat Nanotechnol 7:699–712
3. Cong CX, Shang JZ, Wu X, Cao BC, Peimyoo N, Qiu CY, Sun LT, Yu T (2014) Synthesis and optical properties of large-area single-crystalline 2D semiconductor WS_2 monolayer from chemical vapor deposition. Advanced Optical Materials 2:131–136
4. Yu WJ, Liu Y, Zhou HL, Yin AX, Li Z, Huang Y, Duan XF (2013) Highly efficient gate-tunable photocurrent generation in vertical heterostructures of layered materials. Nat Nanotechnol 8:952–958
5. Choi BK, Lee IH, Kim J, Chang YJ (2017) Tunable wetting property in growth mode-controlled WS_2 thin films. Nanoscale Res Lett 12:262
6. Orofeo CM, Suzuki S, Sekine Y, Hibino H (2014) Scalable synthesis of layer-controlled WS_2 and MoS_2 sheets by sulfurization of thin metal films. Appl Phys Lett 105:1530
7. Gutiérrez HR, Perea-López N, Elías AL, Berkdemir A, Wang B, Lv R, López-Urías F, Crespi VH, Terrones H, Terrones M (2013) Extraordinary room-temperature photoluminescence in triangular WS_2 monolayers. Nano Lett 13:3447–3454
8. Liu KK, Zhang WJ, Lee YH, Lin YC, Chang MT, Su CY, Chang CS, Li H, Shi YM, Zhang H, Lai CS, Li LJ (2012) Growth of large-area and highly crystalline MoS_2 thin layers on insulating substrates. Nano Lett 12:1538–1544
9. Xu ZQ, Zhang YP, Lin SH, Zheng CX, Zhong YL, Xia X, Li ZP, Sophia PJ, Fuhrer MS, Cheng YB, Bao QL (2015) Synthesis and transfer of large-area monolayer WS_2 crystals: moving toward the recyclable use of sapphire substrates. ACS Nano 9:6178–6187
10. Kobayashi Y, Sasaki S, Mori S, Hibino H, Liu Z, Watanabe K, Taniguchi T, Suenaga K, Maniwa Y, Miyata Y (2015) Growth and optical properties of high-quality monolayer WS_2 on graphite. ACS Nano 9:4056–4063
11. Yun SJ, Chae SH, Kim H, Park JC, Park JH, Han GH, Lee JS, Kim SM, Oh HM, Seok J, Jeong MS, Kim KK, Lee YH (2015) Synthesis of centimeter-scale monolayer tungsten disulfide film on gold foils. ACS Nano 9:5510–5519
12. Baek SH, Choi Y, Choi W (2015) Large-area growth of uniform single-layer MoS_2 thin films by chemical vapor deposition. Nanoscale Res Lett 10:388
13. McCreary KM, Hanbicki AT, Jernigan GG, Culbertson JC, Jonker BT (2016) Synthesis of large-area WS_2 monolayers with exceptional photoluminescence. Sci Rep 6:19159
14. Zhang Y, Zhang YF, Ji QQ, Ju J, Yuan HT, Shi JP, Gao T, Ma DL, Liu MX, Chen YB, Song XJ, Hwang HY, Cui Y, Liu ZF (2013) Controlled growth of high-quality monolayer WS_2 layers on sapphire and imaging its grain boundary. ACS Nano 7:8963–8971
15. Li SS, Wang SF, Tang DM, Zhao WJ, Xu HL, Chu LQ, Bando Y, Golberg D, Eda G (2015) Halide-assisted atmospheric pressure growth of large WSe_2 and WS_2 monolayer crystals. Applied Materials Today 1:60–66
16. Kang KN, Godin K, Yang EH (2015) The growth scale and kinetics of WS_2 monolayers under varying H_2 concentration. Sci Rep 5:13205
17. Fu Q, Wang WH, Yang L, Huang J, Zhang JY, Xiang B (2015) Controllable synthesis of high quality monolayer WS_2 on a SiO_2/Si substrate by chemical capor deposition. RSC Adv 5:15795–15799
18. Rong YM, Fan Y, Koh AL, Robertson AW, He K, Wang SS, Tan HJ, Sinclair R, Warner JH (2014) Controlling sulphur precursor addition for large single crystal domains of WS_2. Nanoscale 6:12096–12103
19. van der Vlies AJ, Kishan G, Niemantsverdriet JW, Prins R, Weber T (2002) Basic reaction steps in the sulfidation of crystalline tungsten oxides. J Phys Chem B 106:3449–3457
20. Ohring M (2002) Materials science of thin films-deposition and structure 2nd edition (San Diego, California, USA: Academic Press)
21. Cain JD, Shi FY, Wu JS, Dravid VP (2016) On the growth mechanism of transition metal dichalcogenide monolayers: the role of self-seeding fullerene nuclei. ACS Nano 10:5440–5445
22. Feldman Y, Wasserman E, Srolovitz DJ, Tenne R (1995) High-rate, gas-phase growth of MoS_2 nested inorganic fullerenes and nanotubes. Science 267:222–225
23. Zak A, Feldman Y, Alperovich V, Rosentsveig R, Tenne R (2000) Growth mechanism of MoS_2 fullerene-like nanoparticles by gas-phase synthesis. Journal of American Chemical Society 122:11108–11116
24. Wang SS, Rong YM, Fan Y, Pacios M, Bhaskaran H, He K, Warner JH (2014) Shape evolution of monolayer MoS_2 crystals grown by chemical vapor deposition. Chem Mater 26:6371–6379
25. Thangaraja A, Shinde SM, Kalita G, Tanemura M (2015) Effect of WO_3 precursor and sulfurization process on WS_2 crystals growth by atmospheric pressure CVD. Mater Lett 156:156–160
26. Peimyoo N, Shang JZ, Cong CX, Shen XN, Wu XY, Yeow EKL, Yu T (2013) Nonblinking, intense two-dimensional light emitter: monolayer WS_2 triangles. ACS Nano 7:10985–10994
27. Ma YD, Dai Y, Guo M, Niu CW, Lu JB, Huang BB (2011) Electronic and magnetic properties of perfect, vacancy-doped, and nonmetal adsorbed $MoSe_2$, $MoTe_2$ and WS_2 monolayers. Phys Chem Chem Phys 13:15546–15553
28. Zhao WJ, Ghorannevis Z, Chu LQ, Toh M, Kloc C, Tan PH, Eda G (2013) Evolution of electronic structure in atomically thin sheets of WS_2 and WSe_2. ACS Nano 7:791–797
29. Vega-Mayoral V, Backes C, Hanlon D, Khan U, Gholamvand Z, O'Brien M, Duesberg GS, Gadermaier C, Coleman JN (2016) Photoluminescence from liquid-exfoliated WS_2 monomers in poly(vinyl alcohol) polymer composites. Adv Funct Mater 26:1028–1039